The Aeronautical Journal (2023), **127**, pp. 737–753
doi:10.1017/aer.2022.70

REGULAR PAPER

Enhancing the take-off performance of hypersonic vehicles using the improved chimp optimisation algorithm

X. Zhang[1], J. Yan[1], S. Liu[1] and B. Yan[2,*]

[1]Unmanned System Research Institute, Northwestern Polytechnical University, Xian 710072, China and [2]School of Astronautics, Northwestern Polytechnical University, Xian 710072, China
*Corresponding author. Email: yanbinbin@nwpu.edu.cn

Received: 8 April 2022; **Revised:** 9 June 2022; **Accepted:** 16 June 2022

Keywords: hypersonic vehicle; take-off performance; Chimp Optimisation Algorithm; optimal design

Abstract

The performance of hypersonic vehicles in the take-off stage considerably influences their capability of accomplishing the flight tasks. This study is aimed at enhancing the take-off performance of a cruise aircraft using the improved chimp optimisation algorithm. The proposed algorithm, which uses the Sobol sequence for initial population generation and a function of the weight factors, can effectively overcome the problems of premature convergence and low accuracy of the original algorithm. In particular, the Sobol sequence aims to obtain a better fitness value in the first iteration, and the weight factor aims to accelerate the convergence speed and avoid the local optimal solution. The take-off mass model of the hypersonic vehicle is constructed considering the flight data obtained using the pseudo-spectral method in the climb phase. Simulations are performed to evaluate the algorithm performance, and the results show that the algorithm can rapidly and stably optimise the benchmark function. Compared to the original algorithm, the proposed algorithm requires 28.89% less optimisation time and yields an optimised take-off mass that is 1.72kg smaller.

Nomenclature

x	lateral range [m]
y	longitudinal range [m]
q_d	dynamic pressure [Pa]
h_0	atmospheric density elevation [m]
I_{sp}	impulse [s]
S_r	reference area [m^2]
L	lift force [N]
D	drag force [N]
$mass_1$	fuel consumption in the climb phase [kg]
$mass_2$	initial mass of the aircraft in the cruise phase [kg]
C_D	lift coefficient
C_L	drag coefficient
PLA	throttle value

Greek Symbols

α	angle-of-attack [$\circ$]
γ	flight path angle [$\circ$]
ρ	atmospheric density at sea level [kg/m^3]
μ	random number ranging from 0 to 1

1.0 Introduction

The increasing maturity of scramjet technologies [1] has enabled hypersonic vehicles to fly at a speed of more than Mach 5 in the near space [2, 3]. Owing to such high velocities, high lift-to-drag ratio, long range, and strong manoeuvrability [4, 5, 6], hypersonic vehicles are being increasingly applied in military and civilian fields. The mass of hypersonic vehicles during take-off considerably influences their overall performance. Accurately estimating the take-off mass in the initial stages of the launch mission can help decrease the launch cost and evaluate the effectiveness of various schemes. The resulting enhancement in the overall performance of the aircraft in the take-off stage can facilitate the launch mission [7, 8].

Various take-off performance problems associated with aircraft have been studied considering different application requirements. Dalle et al. [9] proposed a general strategy to determine the minimum take-off mass during the ascent of a generic hypersonic vehicle propelled by a dual-mode ramjet–-scramjet engine with hydrogen fuel. Franco et al. [10] analysed the problem of minimum-fuel cruise at a constant altitude with a fixed arrival time as a singular optimal control problem and attempted to optimise the take-off performance. Ng et al. [11] determined the optimal cruise altitude for an aircraft operating under wind action to minimise the take-off mass. Zhang et al. used a multidisciplinary design optimisation approach to optimise the design of a waverider [12]. However, there remains considerable scope for improvement in solving such optimisation problems.

Swarm intelligence algorithms, as a robust and an adaptable optimisation solution, have attracted considerable research attention [13]. These algorithms are random search algorithms based on biological intelligence or natural phenomena. The core concept is to simulate the foraging and reproduction behaviours of certain social species, abstract these behaviours into quantifiable key indicators, and establish a mathematical model to solve various problems. Duan and Li proposed an artificial-bee-colony-based direct collocation method for the re-entry trajectory optimisation of hypersonic vehicles [14]. The pigeon-inspired optimisation method was used to address the terminal and path constraints [15]. The adaptive grasshopper optimisation algorithm was used [16] to solve the target tracking problem of multiple solar-powered unmanned aerial vehicles (UAVs) in urban environments. Liu and Yan proposed an adaptive simulated annealing particle swarm optimisation (SA-PSO) algorithm to optimise the design parameters of multi-missile formations based on the concept of missile cooperative engagement to maximise the attack effectiveness [17, 18]. Moreover [19], a grey wolf optimisation (GWO)-based algorithm was adopted to determine the optimal UAV trajectory in the presence of moving obstacles. Zhou et al. [20] proposed a parallel genetic algorithm and obtained the global optimisation solution of spacecraft re-entry trajectory. Jiang and Li [21] proposed a hybrid optimisation strategy, in which the PSO and Gauss pseudo-spectral method was used to generate the optimal entry trajectory for Mars pinpoint landing missions.

Overall, several optimisation methods based on the swarm intelligence algorithms and their enhanced variants have been developed, which exhibit certain strengths and limitations in different applications. For example, the stochastic search mechanism in PSO exhibits weak global and local search abilities in early and later iterations, respectively [22]; the GWO exhibits a low population diversity [23]; and the ant colony optimisation involves a large number of parameters [24]. Moreover, all swarm intelligence algorithms typically fall into the local optima, leading to a high computational burden and low accuracy [25, 26].

Khishe et al. [27] recently proposed the chimp optimisation algorithm (ChOA), which is a meta-heuristic optimisation algorithm based on the simulation of chimpanzees' individual intelligence, sexual motivation, and predation behaviours observed in the processes of driving, chasing, and attacking. The ChOA has a simple principle, can be easily implemented, and requires only a few parameters to be adjusted. Consequently, this algorithm has been applied in many fields, such as hybrid energy distribution [28, 29] and medical image recognition [30, 31]. Nevertheless, similar to other swarm intelligence optimisation algorithms, the convergence accuracy and speed of the ChOA must be enhanced.

https://doi.org/10.1017/aer.2022.70 Published online by Cambridge University Press

The advantages of the ChOA make it a promising candidate for optimising the hypersonic vehicle take-off performance. In this study, to explore the applicability of this approach, the ChOA was enhanced and applied to optimise the take-off performance of a hypersonic vehicle. The key contributions of this study can be summarised as follows:

(1) The ChOA tends to easily fall into the local extrema when solving optimisation problems. To address this problem, the Sobol initialisation sequence and weight factor are introduced in the ChOA to increase the convergence rate and facilitate its implementation in engineering practice.

(2) Using the segmented thrust model and aircraft mass model, the take-off performance optimisation problem is converted to a multi-parameter optimisation problem by parameterising the state variables such as the cruise altitude and speed.

(3) To evaluate the performance and accuracy of the improved algorithm, it is applied to optimise ten benchmark functions, and the obtained optimisation results are compared with those of the original ChOA. Considering its validity, rapidity, optimality, and adaptability, the improved ChOA (iwChOA) is applied to optimise the take-off performance of a hypersonic vehicle.

The remaining paper is organised as follows. Section 2 presents the basic theory of the ChOA and improvement strategies. Section 3 describes the modelling of the hypersonic vehicle and its dynamics. Section 4 describes the take-off performance optimisation scheme of the cruise vehicle, aimed at minimising the take-off mass. Section 5 presents the results of the optimisation and comparative analyses. Section 6 presents the concluding remarks.

2.0 Proposed algorithm: iwChOA

2.1 Overview of ChOA

The ChOA is a swarm-based optimisation algorithm inspired by the intelligence and sexual motivation of chimps in their crowd hunting behaviours. A chimp swarm includes four types of chimps: driver, barrier, chaser and attacker, with different skills necessary for a successful hunt. The attacker is the leader of the swarm. The other three types of chimps assist in hunting, and their social status decreases in the order of barrier, chaser and driver. The hunting process can be divided into diversification (exploration) and intensification (exploitation) stages. The exploration stage includes driving, blocking, and chasing, and the exploitation process is focused on attacking the prey. The prey is hunted in both stages. The processes of hunting and chasing the prey can be modelled using Eqs. (1) and (2).

$$\boldsymbol{d} = \left|\boldsymbol{c} \cdot \boldsymbol{x}_{prey}(t) - \boldsymbol{m} \cdot \boldsymbol{x}_{chimp}(t)\right|, \tag{1}$$

$$\boldsymbol{x}_{chimp}(t+1) = \boldsymbol{x}_{prey}(t) - \boldsymbol{a} \cdot \boldsymbol{d}, \tag{2}$$

where t is the number of the current iteration; $\boldsymbol{a}$, $\boldsymbol{m}$, and $\boldsymbol{c}$ are the coefficient vectors; $\boldsymbol{x}_{prey}$ represents the prey position; and $\boldsymbol{x}_{chimp}$ represents the chimp position vector. $\boldsymbol{a}$, $\boldsymbol{m}$, and $\boldsymbol{c}$ can be calculated as

$$\boldsymbol{a} = 2 \cdot f \cdot \boldsymbol{r}_1 - f, \tag{3}$$

$$\boldsymbol{c} = 2 \cdot \boldsymbol{r}_2, \tag{4}$$

$$\boldsymbol{m} = \boldsymbol{Chaotic\_value}, \tag{5}$$

where $\boldsymbol{r}_1$ and $\boldsymbol{r}_2$ are random vectors in the range [0,1]. f is a convergence factor whose value decreases nonlinearly from 2.5 to 0 through the iteration process (in both the exploration and exploitation phases). $\boldsymbol{a}$ is a random vector that determines the distance between the chimps and prey in the range $[-f, f]$. $\boldsymbol{m}$ is a chaotic vector calculated based on various chaotic maps to represent the effect of the sexual motivation of chimps in the hunting process. $\boldsymbol{c}$ is the control coefficient used to describe the chimps' expulsion and

https://doi.org/10.1017/aer.2022.70 Published online by Cambridge University Press

pursuit of prey, defined as a random vector in the range [0,2]. The process of chimps attacking the prey can be modelled using Eqs. (6)–(8).

$$\begin{aligned} \boldsymbol{d}_{Attacker} &= |\boldsymbol{c}_1 \boldsymbol{x}_{Attacker} - \boldsymbol{m}_1 \boldsymbol{x}|\,, \boldsymbol{d}_{Barrier} = |\boldsymbol{c}_2 \boldsymbol{x}_{Barrier} - \boldsymbol{m}_2 \boldsymbol{x}| \\ \boldsymbol{d}_{Chaser} &= |\boldsymbol{c}_3 \boldsymbol{x}_{Chaser} - \boldsymbol{m}_3 \boldsymbol{x}|\,, \boldsymbol{d}_{Driver} = |\boldsymbol{c}_4 \boldsymbol{x}_{Driver} - \boldsymbol{m}_4 \boldsymbol{x}|\,, \end{aligned} \tag{6}$$

$$\begin{aligned} \boldsymbol{x}_1 &= \boldsymbol{x}_{Attacker} - \boldsymbol{a}_1(\boldsymbol{d}_{Attacker}),\ \boldsymbol{x}_2 = \boldsymbol{x}_{Barrier} - \boldsymbol{a}_2(\boldsymbol{d}_{Barrier}) \\ \boldsymbol{x}_3 &= \boldsymbol{x}_{Chaser} - \boldsymbol{a}_3(\boldsymbol{d}_{Chaser}),\ \boldsymbol{x}_4 = \boldsymbol{x}_{Driver} - \boldsymbol{a}_4(\boldsymbol{d}_{Driver}), \end{aligned} \tag{7}$$

$$\boldsymbol{x}(t+1) = \frac{\boldsymbol{x}_1 + \boldsymbol{x}_2 + \boldsymbol{x}_3 + \boldsymbol{x}_4}{4}. \tag{8}$$

As indicated in Eqs. (6)–(8), after population initialisation, four optimal solutions are selected to define the positions of the attackers, barriers, chasers, and drivers. The positions of other chimps in the population are updated considering these positions. In other words, the position of the prey is estimated by those of the four best individuals, and the locations of other chimps are randomly updated in the vicinity.

In the last stage of hunting, the individuals achieve food satisfaction and exhibit natural wild behaviour in the presence of social opportunities. Specifically, the chimps attempt to obtain food by force and chaos. The chaotic behaviour of chimps in the final stage helps alleviate the problems of local optimum trapping and low convergence speed, and chaotic maps can be used to enhance the ChOA performance. The updating process is modelled using Eq. (9), where μ is a random number in [0,1]. Because certain chimps may not have any sexual motivation in the hunting process, a probability of 50% is set to determine whether the position update strategy of the chimps is normal (Eq. (2)) or chaotic (Eq. (9)). The process flow of the ChOA is illustrated in Fig. 1.

$$\boldsymbol{x}_{chimp}(t+1) = \begin{cases} \boldsymbol{x}_{\text{prey}}(t) - \boldsymbol{a} \cdot \boldsymbol{d} & if\ \mu < 0.5 \\ \boldsymbol{Chaotic\_value} & if\ \mu > 0.5 \end{cases}. \tag{9}$$

2.2 Improved ChOA

Although the ChOA has many advantages and has been applied in many fields, it has a few limitations. Specifically, the population initialisation is based on random distribution, which leads to a low population diversity, aimlessness in the individual early search, and low convergence speed of the algorithm. In addition, because the positions of the other chimps are updated based on those of the attackers, these chimps may be trapped in the local optimum, which limits their exploration of new areas in the search space owing to their solution space being concentrated around the attackers' solutions.

Consequently, the original approach is not suitable for solving highly complex optimisation problems owing to limitations such as low diversity, vulnerability to local optimum trapping, and low convergence speed. To address these limitations, the population initialisation and location update methods are enhanced in this study. To enhance the exploitation phase of the standard ChOA, the search process equations are modified, as described in the following subsections.

2.2.1 Sobol sequence for population initialisation

For all algorithms involving sampling, a superior sample distribution can be obtained using evenly distributed random numbers. In the original ChOA, the population initialisation process is based on random distribution, which leads to a low diversity and aimlessness of individual optimisation. In the improved algorithm, the Sobol sequence is used to initialise the population. The dimensions of the Sobol sequence are based on radical inversion with a factor of 2; however, each dimension has a specific generation

https://doi.org/10.1017/aer.2022.70 Published online by Cambridge University Press

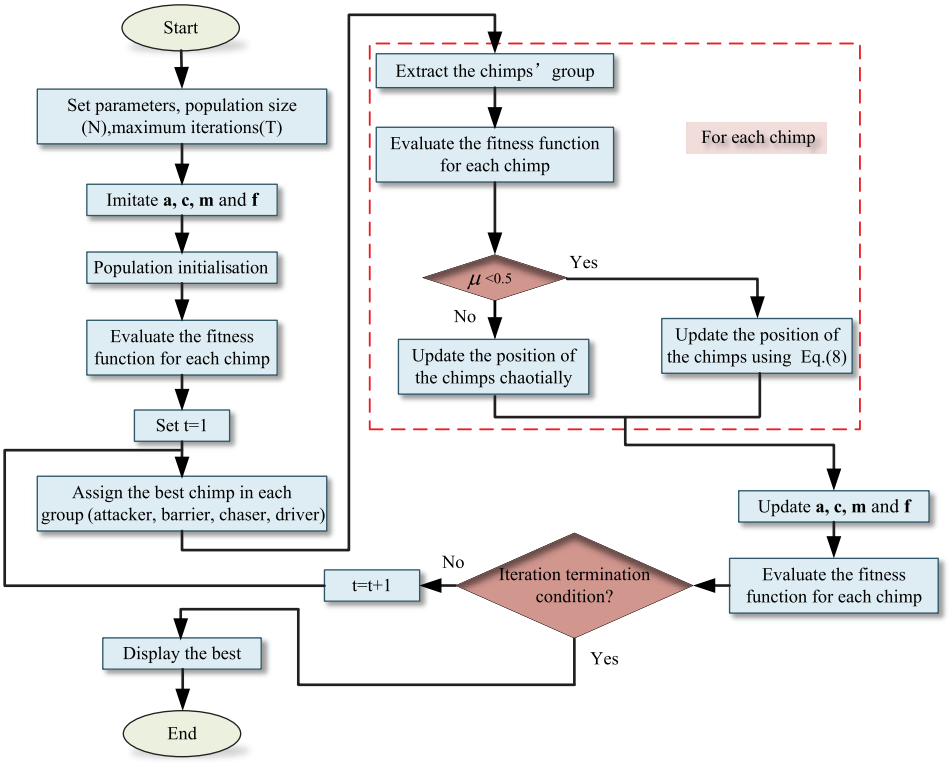

Figure 1. *Process flow of ChOA.*

matrix. Notably, the Sobol sequence is a low discrepancy sequence, in which a deterministic pseudo-random number sequence is used to replace the pseudo-random number sequence to fill the sample space as evenly as possible. Therefore, the Sobol sequence is associated with a high computational efficiency and wide coverage of sampling points in solving the initial sampling problems.

Considering the optimisation problem of interest, the upper and lower limits of the two-dimensional space are set as $\boldsymbol{lb} = [5\ 25{,}000]$ and $\boldsymbol{ub} = [6\ 30{,}000]$ to describe the cruise state. The random number in the sampling space is generated using Eq. (10), and the population size is set as 30. S_i is the ith random number generated by the Sobol sequence in the range [0,1].

$$\boldsymbol{X_n} = \boldsymbol{lb} + S_i \cdot (\boldsymbol{ub}\text{-}\boldsymbol{lb}). \tag{10}$$

2.2.2 Weight factor

To alleviate the problem of the other chimps falling into the local optimum, the iwChOA incorporates a position-weighted relationship based on a weight factor that can be mathematically formulated as follows:

$$\beta_1 = \frac{|\boldsymbol{x}|_1}{|\boldsymbol{x}|_1 + |\boldsymbol{x}|_2 + |\boldsymbol{x}|_3 + |\boldsymbol{x}|_4}, \tag{11}$$

$$\beta_2 = \frac{|\boldsymbol{x}|_2}{|\boldsymbol{x}|_1 + |\boldsymbol{x}|_2 + |\boldsymbol{x}|_3 + |\boldsymbol{x}|_4}, \tag{12}$$

https://doi.org/10.1017/aer.2022.70 Published online by Cambridge University Press

$$\beta_3 = \frac{|\boldsymbol{x}|_3}{|\boldsymbol{x}|_1 + |\boldsymbol{x}|_2 + |\boldsymbol{x}|_3 + |\boldsymbol{x}|_4}, \tag{13}$$

$$\beta_4 = \frac{|\boldsymbol{x}|_4}{|\boldsymbol{x}|_1 + |\boldsymbol{x}|_2 + |\boldsymbol{x}|_3 + |\boldsymbol{x}|_4}, \tag{14}$$

$$\boldsymbol{x}(t+1) = \frac{1}{\beta_1 + \beta_2 + \beta_3 + \beta_4} \times \frac{\beta_1|\boldsymbol{x}|_1 + \beta_2|\boldsymbol{x}|_2 + \beta_3|\boldsymbol{x}|_3 + \beta_4|\boldsymbol{x}|_4}{4}. \tag{15}$$

The learning rate is introduced in Eq. (8) to obtain Eq. (15). β_1, β_2, β_3, and β_4 are the learning rates of other chimps with respect to the attacker, barrier, chaser and driver, respectively, in terms of the Euclidean distances. The dynamic learning rate in Eq. (15) varies across iterations, which helps increase the convergence speed and ensure the avoidance of the local optima in scenarios in which the attackers, barriers, chasers and drivers are less likely to know the position of the prey.

2.2.3 iwChOA implementation

The implementation of the iwChOA involves the following steps:

Step 1: Initialise the chimp colony, including the number of individuals in the population, N, maximum number of iterations, T, dimension d, and limits of the search space, $\boldsymbol{lb}$ and $\boldsymbol{ub}$, using the Sobol sequence and set the relevant parameters;

Step 2: Calculate the fitness value of each chimp individual. Identify the first four individual positions with the lowest fitness and define them as $\boldsymbol{x}_{Attacker}$, $\boldsymbol{x}_{Barrier}$, $\boldsymbol{x}_{Chaster}$ and $\boldsymbol{x}_{Driver}$.

Step 3: Update the parameters $\boldsymbol{a}$ and $\boldsymbol{c}$ according to Eqs. (3) and (4).

Step 4: Update $\boldsymbol{x}_{Attacker}$, $\boldsymbol{x}_{Barrier}$, $\boldsymbol{x}_{Chaster}$ and $\boldsymbol{x}_{Driver}$ according to Eqs. (6),(7), and(9), and update the locations of the chimp population according to Eqs. (11)–(15).

Step 5: Establish the chaotic maps based on Eq. (5).

Step 6: Repeat Steps 3 to 5 until the maximum number of iterations is reached or the algorithm converges to the required accuracy.

Step 7: Output the global optimal position $\boldsymbol{x}_{Attacker}$.

3.0 Vehicle model

A hypersonic cruise vehicle must be able to cruise in hypersonic flow for a reasonable duration [32]. The hypersonic cruise vehicle considered in this study is assumed to be propelled by a scramjet and operate in a still atmosphere. This section describes the modelling of the hypersonic cruise vehicle, including the equations of motion and thrust and aerodynamic expressions.

A six-degree-of-freedom (DOF) winged-cone hypersonic vehicle model, shown in Fig. 2, is selected to demonstrate the reliability of the proposed optimisation scheme. The body and propulsion system are integrated, and the vehicle consists of four control surfaces: right elevon, left elevon, rudder and canard. The influence of the rudder and canard is ignored. The model parameters can be found in a previous report [33].

3.1 Dynamics model

For simplicity, the following assumptions are implemented:

(1) The curvature of the earth is ignored, and the ground coordinate system is the inertial coordinate system.

(2) The instantaneous equilibrium hypothesis is applied.

(3) Only longitudinal motion is considered.

https://doi.org/10.1017/aer.2022.70 Published online by Cambridge University Press

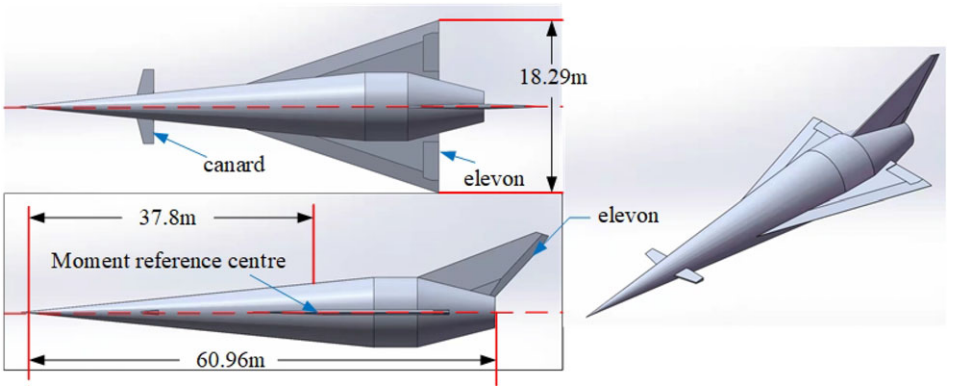

Figure 2. *Winged-cone configuration.*

Equations (16)–(21) represent a typical dynamic model of a hypersonic vehicle:

$$\frac{dV}{dt} = \frac{T\cos\alpha - D}{m} - g\sin\gamma, \tag{16}$$

$$\frac{d\gamma}{dt} = \frac{L + T\sin\alpha}{m} - \frac{g}{V}\cos\gamma, \tag{17}$$

$$\frac{d\alpha}{dt} = q_d - \frac{d\gamma}{dt}, \tag{18}$$

$$\frac{dx}{dt} = V\cos\gamma, \tag{19}$$

$$\frac{dy}{dt} = V\sin\gamma, \tag{20}$$

$$\frac{dm}{dt} = -T/(g \cdot isp), \tag{21}$$

where $g = g_0(\frac{R_e}{r})^2$ is the acceleration due to gravity, g_0 is the acceleration due to gravity on the ground, and R_e is the radius of the Earth. D and L are the drag and lift forces, respectively, calculated as

$$D = q_d S_r C_D, \tag{22}$$

$$L = q_d S_r C_L. \tag{23}$$

The dynamic pressure q_d can be defined as

$$q_d = \frac{1}{2}\rho v^2, \tag{24}$$

ρ is the atmospheric density, which can be calculated as

$$\rho = \rho_0 e^{((r-R_e)/h_0)}, \tag{25}$$

where ρ_0 is the atmospheric density at sea level (1.225570827014494), and h_0 is the elevation at which the density is being evaluated (7254.24).

https://doi.org/10.1017/aer.2022.70 Published online by Cambridge University Press

Table 1. *Engine specific impulse values*

ψ	Mach 4	Mach 6	Mach 8	Mach 10	Mach 15	Mach 20	Mach 25
0	3, 600	2, 800	2, 200	1, 800	1, 300	1, 300	900
0.5	3, 600	2, 800	2, 200	1, 800	1, 300	1, 300	900
1	3, 400	2, 800	2, 200	1, 800	1, 300	1, 300	900
3	3, 000	2, 700	1, 300	800	620	700	600
5	800	1, 900	1, 000	600	470	540	520
10	100	100	100	100	100	100	100

3.2 Hypersonic cruise vehicle model

The considered model adopts three engines in hypersonic cruise flight, which operate in a combined cycle propulsion system. Such power plants can cover the mission requirements in different speed ranges such as low speed, supersonic and hypersonic regimes [33]. The ratio of the engine thrust to the Mach number can be calculated using the following analytical formulas.

$$\begin{cases} 0.0 \le Mach \le 2.0 \\ T = PLA * (2.99 * 10^5 - 32.8 * (h) + 1.43 * 10^{-3} * (h)^2 - 2.29 * 10^{-8} * (h)^3, \\ \qquad + 3.75 * 10^3 * (Mach)^3) \end{cases} \tag{26}$$

$$\begin{cases} 2.0 \le Mach \le 5.0 \\ T = PLA * (396.103 * Mach - 703.1 * Mach^2 + 816.19 * Mach^3 - 442.48 * Mach^4, \\ \qquad + 118.28 * Mach^5 - 15.34 * Mach^6 + 0.772 * Mach^7) * 5 * 10^3; \end{cases} \tag{27}$$

$$\begin{cases} 5.0 \le Mach \le 6.0 \\ T = PLA * (396.103 * Mach - 703.1 * Mach^2 + 816.19 * Mach^3 - 442.48 * Mach^4. \\ \qquad + 118.28 * Mach^5 - 15.34 * Mach^6 + 0.772 * Mach^7) * 5 * 10^3; \end{cases} \tag{28}$$

The change in the hypersonic vehicle mass during flight, which depends on the thrust, gravitational acceleration and specific impulse, can be obtained using Eq. (21). The specific impulse can be obtained via interpolation of the data in Table 1.

The aerodynamics parameters are obtained via piecewise calculation [33]:

$$C_D = f_D(Mach, \alpha), \tag{29}$$

$$C_L = f_L(Mach, \alpha), \tag{30}$$

where f_D and f_L are piecewise interpolation functions to analyse the drag and lift coefficients, respectively.

4.0 Take-off mass optimisation problem

4.1 Objective function

As a key phase of the trajectory, the cruise phase has its own objectives. The take-off performance optimisation problem of a hypersonic vehicle pertains to determining the optimal cruise speed and altitude, $\boldsymbol{S}^*(t) = [M^*(t), A^*(t)]$, to minimise the take-off mass subject to range requirements and other constraints. Typically, the objective function is required to be maximised. Therefore, the negative take-off mass is set as the performance index:

$$J(s) = -\left|mass_1 + mass_2\right|, \tag{31}$$

where $mass_1$ is the weight of the fuel consumed in the climb phase, and $mass_2$ is the initial mass of the vehicle in the cruise phase. The optimisation objective is to determine the best cruise state to maximise

https://doi.org/10.1017/aer.2022.70 Published online by Cambridge University Press

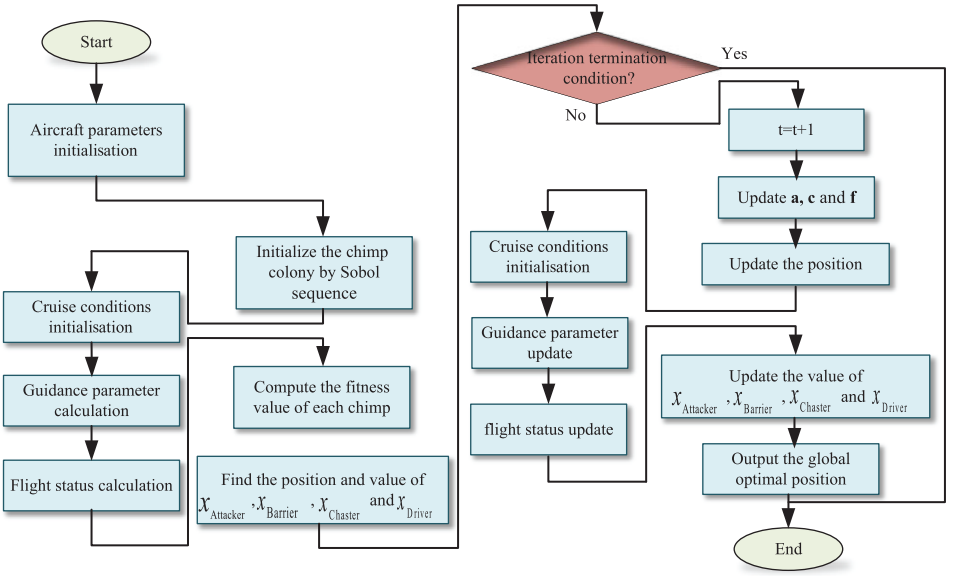

Figure 3. *Optimisation of the take-off mass.*

the objective function specified in Eq. (31), subject to the 3-DOF dynamics presented in Eqs. (16)–(21) and constraint conditions.

4.2 Constraints

The trajectory optimisation of a hypersonic vehicle in the climb phase is a typical nonlinear optimal control problem with state and control constraints. The Gaussian pseudo-spectral method can obtain a superior solution with a lower computational cost. Therefore, the flight process in the climb phase is modelled using the Gauss pseudo-spectral method [34]. In the optimisation process, the initial speed and altitude in the climb phase are set as $v_0 = 100$m/s and $h_0 = 50$m, respectively. The end of the climb phase marks the start of the cruise phase, which is the search space in this study. In this phase, the Mach number is $M = [5, 6]$ and altitude is $A = [25,000, 30,000]$. The search space is divided equally, and certain points are selected as the end points of the climb phase. The Gauss pseudo-spectral method is used to determine the changes in the flight state variables in the climb process, with the variable of interest being the vehicle mass.

As mentioned earlier, the objective of the considered problem is to determine the optimal cruise speed and altitude to minimise the aircraft take-off mass. The main requirement for aircraft control in the cruise phase is to maintain stable flight and satisfy the range requirements. Because the state variables in the cruise phase change gradually, flight control can be realised in a facile manner. The stability of the trajectory in the cruise phase must be ensured through guidance control, which mainly involves altitude and speed control, the control variables of which are the angle-of-attack and throttle equivalent, respectively. In this study, the classic proportional integral–derivative (PID) control is adopted for cruise control, although the details are not presented in this paper.

The cruise flight process contains four control constraints and two path constraints, as indicated in Eq. (32). All constraints except for one are inequality constraints. The equality constraint ensures that the vehicle attains the cruise range. The inequality constraints ensure that the change in the angle-of-attack and throttle equivalent do not exceed the pre-programmed boundaries, and the rate of change of the attack angle does not exceed the limits. The range, angle-of-attack and rate of change of the angle-of-attack are expressed in units of m, deg and deg/s, respectively, and the fuel equivalent is expressed as a percent point. The path constraint ensures that the dynamic pressure and heat flux density of the

https://doi.org/10.1017/aer.2022.70 Published online by Cambridge University Press

Table 2. *Benchmark functions used in the experiments*

Name	Function	Range	$f_{\min}$
Sphere	$F_1(x) = \sum_{i=1}^{n} x_i^2$	[–100,100]	0
Schwefel.2.21	$F_2(x) = \max_i\{\lvert x_i\rvert, 1 \le i \le n\}$	[–100,100]	0
Rosenbrock	$F_3(x) = \sum_{i=1}^{n-1} [100(x_{i-1} - x_i^2)^2 + (x_i - 1)^2]$	[–30,30]	0
QuarticWN	$F_4(x) = \sum_{i=1}^{n} ix^4 + random\,[0, 1)$	[–1.28,1.28]	
Griewank	$F_5(x) = \frac{1}{4000}\sum_{i=1}^{n} x_i^n - \prod_{i=1}^{n} \cos\left(\frac{x_i}{\sqrt{i}}\right) + 1$	[–600,600]	0
Penalised1	$F_6(x) = \frac{\pi}{n}\{10\sin(\pi y_1) + \sum_{i=1}^{n-1}(y_i - 1)^2[1 + 10\sin^2(\pi y_{i+1})] + (y_n - 1)^2\} + \sum_{i=1}^{n} u(x_i, 10, 100, 4), y_i = 1 + \frac{1}{4}(x_i + 1)$ $u(x_i, a, k, m) = \begin{cases} k(x_i - a)^m & x_i > a \\ 0 & -a < x_i < a \\ k(-x_i - a)^m & x_i < -a \end{cases}$	[–50,50]	0
Penalised2	$F_7(x) = \frac{1}{10}\{\sin^2(3\pi x_1) + \sum_{i=1}^{n-1}(x_i - 1)^2[1 + \sin^2(3\pi x_{i+1})] + (x_n - 1)^2[1 + \sin^2(2\pi x_{i+1})]\} + \sum_{i=1}^{n} u(x_i, 5, 100, 4)$	[–50,50]	0
Rastrigin	$F_8(x) = \sum_{i=1}^{n} [x_i^2 - 10\cos(2\pi x_i) + 10]$	[–5.12,5.12]	0
Shekel's Foxholes Function	$F_9(x) = \left(\frac{1}{500} + \sum_{j=1}^{25} \frac{1}{j + \sum_{i=1}^{2}(x_i - a_{ij})^6}\right)^{-1}$	[–65,65]	1
Hatman's Function1	$F_{10}(x) = -\sum_{i=1}^{4} c_i \exp\left(-\sum_{j=1}^{3} a_{ij}(x_j - p_{ij})^2\right)$	[0,1]	–3.86

vehicle do not exceed the maximum limits.

$$\begin{cases} Range = 1.3 * 10^7 \\ 0 \le \alpha \le 10, -3 \le \dot{\alpha} \le 3, 0 \le PLA \le 100\% \\ q = \frac{1}{2}\rho V^2 \le q_{\max}, \dot{q}_s = k_p \rho^{0.5} V^{3.08} \le \dot{q}_{s\max} \end{cases}. \tag{32}$$

4.3 Optimisation based on iwChOA

The take-off performance optimisation process based on the iwChOA is illustrated in Fig. 3. First, the parameters of the aircraft and proposed algorithm are initialised, and the fitness of the initial population is calculated. The iwChOA continuously updates the position according to the process described in Section 2.2.3 until the optimisation result satisfies the iteration termination conditions. The fitness value is obtained by calculating the flight state of the aircraft, which is the take-off mass when the flight range is attained.

5.0 Results and discussion

Unless specified otherwise, all the numerical results presented in this paper have been generated using a computer with an Intel i7-11800H processor (2.3 GHz, eight cores, 16 threads), a 16.0 GB memory, and Windows operating system.

5.1 Benchmark function test

The performance and accuracy of the iwChOA are evaluated by using it to optimise ten benchmark functions, listed in Table 2, and comparing the obtained results with those of the original ChOA.

The benchmark functions used in the experiment have different properties. Specifically, $F_1(x)$ to $F_4(x)$ are unimodal functions, $F_5(x)$ to $F_8(x)$ are complex multimodal functions, and $F_9(x)$ and $F_{10}(x)$ are fixed-dimension multimodal function.

https://doi.org/10.1017/aer.2022.70 Published online by Cambridge University Press

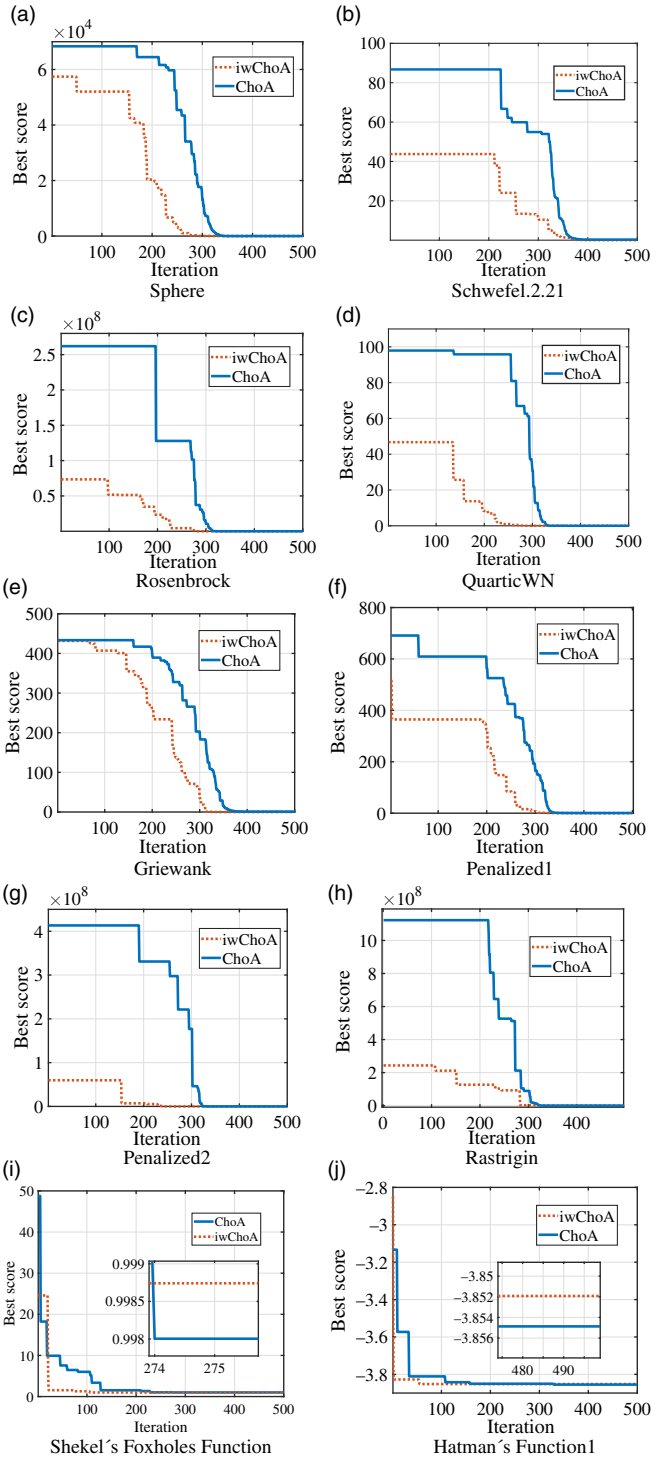

Figure 4. *Benchmark function optimisation results.*

https://doi.org/10.1017/aer.2022.70 Published online by Cambridge University Press

Table 3. *Benchmark function optimisation results*

Function	Algorithm	Optimal value	Average value	Standard deviation
$F_1(x)$	ChOA	1.47×10^{-23}	3.31×10^{-13}	5.62×10^{-13}
	iwChOA	0	0	0
$F_2(x)$	ChOA	3.41×10^{-7}	4.85×10^{-3}	3.61×10^{-3}
	iwChOA	6.53×10^{-17}	3.53×10^{-11}	5.28×10^{-12}
$F_3(x)$	ChOA	2.78×10^{1}	2.82×10^{1}	2.19×10^{-1}
	iwChOA	2.23×10^{1}	2.47×10^{1}	7.39×10^{-2}
$F_4(x)$	ChOA	4.83×10^{-5}	3.67×10^{-4}	2.32×10^{-4}
	iwChOA	1.45×10^{-5}	1.73×10^{-5}	1.62×10^{-5}
$F_5(x)$	ChOA	2.54×10^{-11}	1.62×10^{-2}	1.73×10^{-2}
	iwChOA	0	0	0
$F_6(x)$	ChOA	2.98×10^{-2}	3.65×10^{-1}	5.57×10^{-9}
	iwChOA	4.36×10^{-7}	5.49×10^{-4}	3.72×10^{-11}
$F_7(x)$	ChOA	3.34×10^{-2}	5.57×10^{-1}	2.73×10^{-1}
	iwChOA	1.83×10^{-9}	2.84×10^{-6}	1.70×10^{-5}
$F_8(x)$	ChOA	3.72×10^{-13}	2.25×10^{0}	3.64×10^{0}
	iwChOA	0	0	0
$F_9(x)$	ChOA	9.98×10^{-1}	9.98×10^{-1}	1.83×10^{-5}
	iwChOA	9.99×10^{-1}	9.99×10^{-1}	1.70×10^{-5}
$F_{10}(x)$	ChOA	-3.85×10^{0}	-3.85×10^{0}	3.53×10^{-6}
	iwChOA	-3.86×10^{0}	-3.86×10^{0}	2.59×10^{-9}

The parameters of the original and proposed algorithms are set as follows: The population size, N, is 30, and the maximum number of iterations, T, is 500. Each function is implemented thirty times independently, and the average and standard deviation are obtained. Figure 4 and Table 3 present the optimisation results of the two algorithms for different benchmark functions. In Table 3, the optimal values indicate the optimisation ability of the algorithm, the average values reflect the convergence accuracy, and the standard deviation reflects the robustness and stability of the algorithm.

The experimental results demonstrate that the iwChoa outperforms the original algorithm in terms of the optimisation ability for unimodal and multimodal functions. For $F_1(x)$, $F_5(x)$, and $F_8(x)$, iwChOA exhibits a superior optimisation performance; it can directly find the optimal value of zero. In addition to a high convergence accuracy, the iwChOA exhibits an enhanced convergence speed, attributable to the better initial value determined using the Sobol sequence and enhancement in the position update speed owing to the use of the weight factor.

5.2 Analysis of vehicle mass in the climb phase

The Gaussian pseudo-spectrum method is used to perform the optimisation in the climb phase. Figure 5 shows the changes in several state quantities, including the altitude, speed, mass and angle-of-attack when the winged-cone hypersonic vehicle climbs to three example points. The end of the climb phase marks the starting point of the cruise trajectory. $mass_1$ in the objective function can be obtained through a simulation analysis of the climb phase. At the end of one iteration, the initial mass of the vehicle in the cruise phase, $mass_2$, is calculated. The objective function is the sum of $mass_1$ and $mass_2$.

5.3 Analysis of optimisation results based on iwChOA

The ChOA in which only the Sobol sequence is introduced is denoted as iChOA. The performances of the proposed iwChOA and conventional ChOA in solving the problem described in Section 4 are compared.

https://doi.org/10.1017/aer.2022.70 Published online by Cambridge University Press

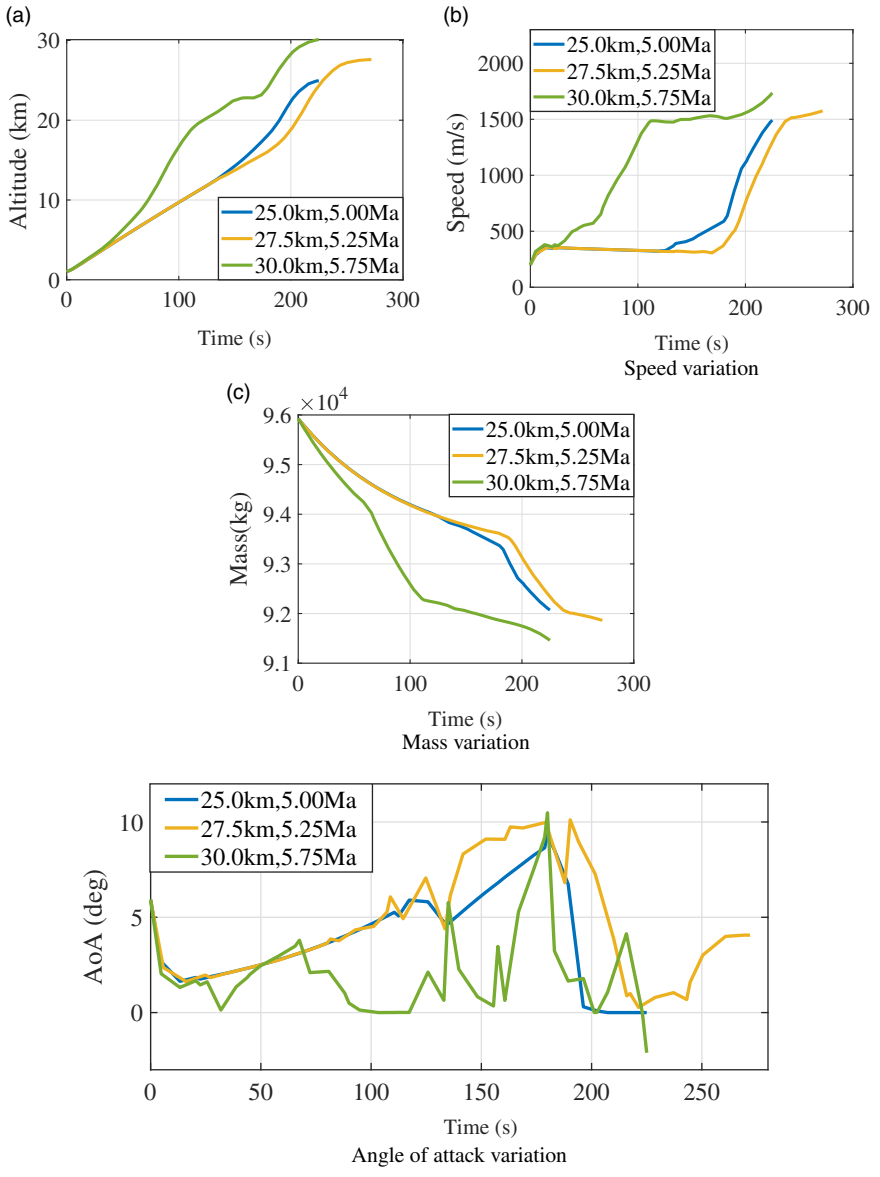

Figure 5. *Analysis of vehicle mass in the climb phase.*

The comparative analysis involves three evaluation indexes: population initialisation, objective function accuracy, and calculation time. For both the algorithms, the swarm size is 30, and the maximum number of iterations is 100. First, the position distributions of the first-generation population initialised using the Sobol sequence are compared with those calculated using the original algorithm. As shown in Fig. 6, the position distribution attained using the Sobol sequence is more uniform, which helps obtain a better position of the attackers after the first iteration. Figure 7 shows the relationship between the fitness and number of iterations in the optimisation process for the original ChOA, iChOA, and iwChOA, with the fitness corresponding to the take-off mass. All three algorithms can solve the take-off mass optimisation problem. The iChOA and iwChOA exhibit the same initial fitness owing to the use of the Sobol sequence;

https://doi.org/10.1017/aer.2022.70 Published online by Cambridge University Press

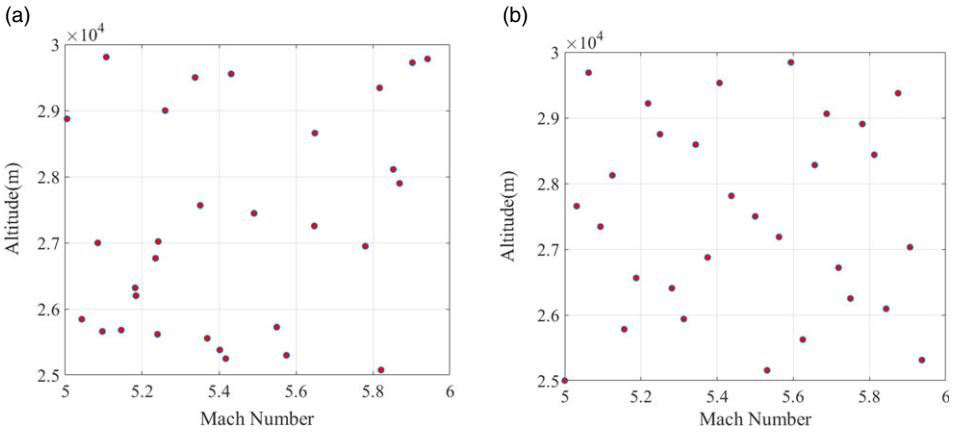

Figure 6. *Population initialisation results.*

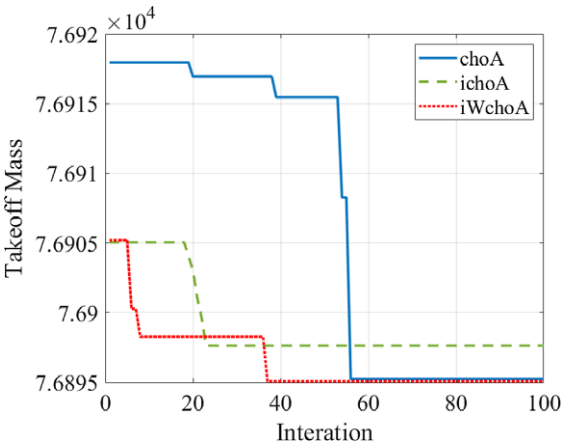

Figure 7. *Comparison of optimisation process.*

however, the convergence accuracy of the iChOA is lower. The lower accuracy is attributable to the fact that the smaller initial fitness decreases the population diversity, which causes the iterative process to fall into the local optima and remain in this state for a considerable period. Moreover, the iwChOA considerably outperforms the ChOA because the weight factor guides the population to determine the global optimal solution in a stable manner, thereby enhancing the convergence accuracy and speed of the iwChOA.

The optimal cruise Mach numbers determined by the ChOA and iwChOA are approximately 5.87 and 5.85, respectively. Because of this difference in the Mach numbers, the optimisation curves of the two algorithms in Fig. 6 do not coincide, and the optimal take-off mass determined by the iwChOA is 1.72kg smaller than that obtained using the ChOA. Both algorithms yield the best cruising altitude as 30 km.

Figure 8 shows the runtime of the ChOA and iwChOA. The optimisation process is repeated 100 times, and the runtime of the two algorithms in each iteration is obtained. The positions of thirty chimps are updated after every iteration. The ChOA and iwChOA require, on average, 216.1 and 230.5s to

https://doi.org/10.1017/aer.2022.70 Published online by Cambridge University Press

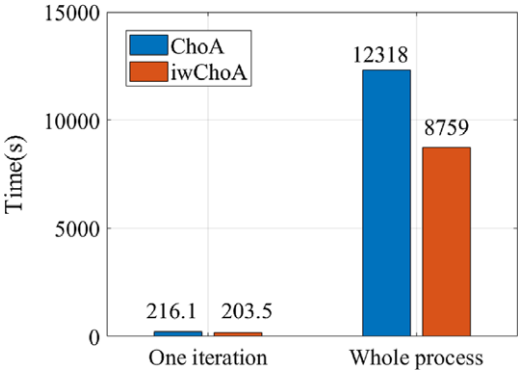

Figure 8. *Comparison of the algorithm runtime.*

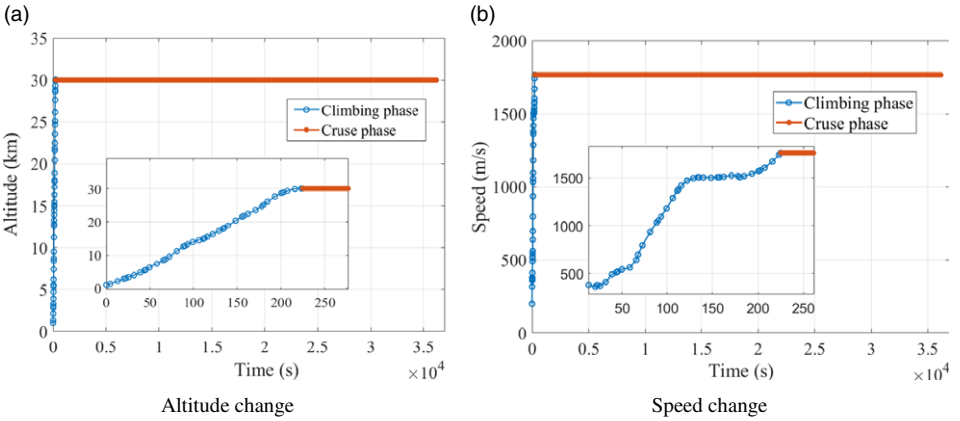

Figure 9. *Optimal trajectory for winged-cone hypersonic vehicle.*

complete each iteration, respectively. Notably, the iwChOA requires fewer iterations to solve the cruise trajectory optimisation problem of the winged-cone hypersonic vehicle and thus, consumes 28.89% less time than the original algorithm.

5.4 Take-off performance optimisation

Figure 9 shows the trajectory of the hypersonic vehicle corresponding to the optimal take-off performance. The flight altitude and speed when the flight phase changes from climb to cruise at the best cruise point are shown in Figs. 9(a) and (b), respectively.

6.0 Conclusions

The ChOA is improved by incorporating the Sobol sequence and weight factor to enhance the take-off performance of a hypersonic cruise vehicle. The flight states in the climb and cruise phases are considered to determine the optimal take-off mass of the vehicle. The simulation results demonstrate that the proposed algorithm can better optimise ten benchmark functions compared to the original algorithm. Moreover, the iwChOA outperforms the original algorithm in solving the take-off performance optimisation problem, owing to its rapid convergence, high accuracy and adaptability. The take-off

https://doi.org/10.1017/aer.2022.70 Published online by Cambridge University Press

mass determined using the proposed algorithm is 1.72kg smaller than that obtained using the original algorithm, and the runtime is 28.89% lower.

Future studies can be aimed at considering the attitude dynamics, which were not considered in this study.

Acknowledgements. The authors appreciate the financial support from the Natural Science Basic Research Plan in Shaanxi Province of China (Grant No. 2020JC-19), the National Natural Science Foundation of China (NSFC) (Grant NO. 62173274) and the Natural Science Foundation of Shaanxi Province (Grant NO. 2020JQ-219).

References

[1] Huang, W., Du, Z., Yan, L. and Moradi, R. Flame propagation and stabilization in dual-mode scramjet combustors: A survey, *Prog. Aerosp. Sci.*, 2018, **101**, pp 13–30.
[2] Zhao, Z., Huang, W., Yan, L. and Yang, Y. An overview of research on wide-speed range waverider configuration, *Prog. Aerosp. Sci.*, 2020, **113**, pp 1–14.
[3] Liu, S., Yan, B., Zhang, T., Zhang, X. and Yan, J. Coverage-based cooperative guidance law for intercepting hypersonic vehicles with overload constraint, *Aerospace Science and Technology*, 2022, **126**, 107651. doi:10.1016/j.ast.2022.107651.
[4] Han, T., Hu, Q., Shin, H., Tsourdos, A. and Xin, M. Sensor-based robust incremental three-dimensional guidance law with terminal angle constraint, *J. Guid. Cont. Dynam.*, 2021, **44**, (11), pp 2016–2030.
[5] Han, T., Shin, H., Hu, Q., Tsourdos, A. and Xin, M. Differentiator-based incremental three-dimensional terminal angle guidance with enhanced robustness, *IEEE Trans. Aerosp. Electron. Syst.*, 2022, Published Online, doi:10.1109/TAES.2022.3158639.
[6] Han, T., Hu, Q. and Xin, M. Three-dimensional approach angle guidance under varying velocity and field-of-view limit without using line-of-sight rate, *IEEE Trans. Syst. Man Cybern. Syst.*, 2022, Published Online, doi:10.1109/TSMC.2022.3150299.
[7] Liu, S., Yan, B., Zhang, X., Liu, W. and Yan, J. Fractional-order sliding mode guidance law for intercepting hypersonic vehicles, *Aerospace*, 2022, **9**, (2), pp 53–69.
[8] Liu, S., Yan, B., Liu, R., Dai, P., Yan, J. and Xin, G. Cooperative guidance law for intercepting a hypersonic target with impact angle constraint, *Aeronaut. J.*, 2022, **126**, (1300), pp 1026–1044.
[9] Dalle, D.J., Torrez, S.M., Driscoll, J.F., Bolender, M.A. and Bowcutt, K.G. Minimum-fuel ascent of a hypersonic vehicle using surrogate optimisation, *J. Aircr.*, 2014, **51**, (6), pp 1973–1986.
[10] Franco, A., Rivas, D. and Valenzuela, A. Minimum-fuel cruise at constant altitude with fixed arrival time, *J. Guid. Cont. Dynam.*, 2010, **33**, (1), pp 280–285.
[11] Ng, H.K., Sridhar, B. and Grabbe, S. Optimising aircraft trajectories with multiple cruise altitudes in the presence of winds, *J. Aerosp. Inform. Syst.*, 2014, **11**, (1), pp 35–47.
[12] Zhang, T., Yan, X., Huang, W., Che, X. and Wang, Z. Multidisciplinary design optimisation of a wide speed range vehicle with waveride airframe and RBCC engine, *Energy*, 2021, **235**, pp 1–14.
[13] An, K., Guo, Z.Y., Xu, X.P. and Huang, W. A framework of trajectory design and optimisation for the hypersonic gliding vehicle, *Aerosp. Sci. Technol.*, 2020, **106**, (110), pp 1–11.
[14] Duan, H., and Li, S. Artificial bee colony-based direct collocation for reentry trajectory optimisation of hypersonic vehicle, *IEEE Trans. Aerosp. Electron. Syst.*, 2015, **51**, (1), pp 615–626.
[15] Sushnigdha, G. and Joshi, A. Re-entry trajectory optimization using pigeon inspired optimization based control profiles, *Advances in Space Research*, 2018, **62**, (11), pp 3170–3186.
[16] Wu, J., Wang, Wang., Li, N. Yao, P., Huang, Y., Su, Z. and Yu, Y. Distributed trajectory optimisation for multiple solar-powered UAVs target tracking in urban environment by adaptive grasshopper optimisation algorithm, *Aerosp. Sci. Technol*, 2017, **70**, pp 497–510.
[17] Liu, S., Huang, F., Yan, B., Zhang, T., Liu, R. and Liu, W. Optimal design of multimissile formation based on an adaptive SA-PSO algorithm, *Aerospace*, 2022, **9**, (1), pp 1–15.
[18] Liu, S., Liu, W., Huang, F., Yin, Y., Yan, B. and Zhang, T. Multitarget allocation strategy based on adaptive SA-PSO algorithm, *Aeronaut. J.*, 2022, **126**, (1300), pp 1069–1081.
[19] Radmanesh, M., Kumar, M. and Sarim, M. Grey wolf optimisation based sense and avoid algorithm in a Bayesian framework for multiple UAV path planning in an uncertain environment, *Aerosp. Sci. Technol.*, 2018, **77**, pp 168–179.
[20] Zhou, W., Ma, H., Wu, Z. and Yin, K. Parallel genetic algorithm applied to spacecraft reentry trajectory, *Practical Applications of Intelligent Systems, Springer*, 2014, **279**, pp 867–875.
[21] Jiang, X., and Li, S. Mars atmospheric entry trajectory optimisation via particle swarm optimisation and Gauss pseudo-spectral method, *Proc. Inst. Mech. Eng. G J. Aerosp. Eng.*, 2016, **230**,(12) pp 2320–2329.
[22] Imran, M., Hashim, R. and Khalid, N.E.A. An overview of particle swarm optimisation variants, *Proc. Eng.*, 2016, **53** pp 491–496.
[23] Skinderowicz, R. Improving ant colony optimisation efficiency for solving large TSP instances, *Appl. Soft Comput.*, 2022, **120** pp 1–15.
[24] Nadimi-Shahraki, M.H., Taghian, S., Mirjalili, S., Zamani, H. and Bahreininejad, A. GGWO: Gaze cues learning-based grey wolf optimiser and its applications for solving engineering problems, *J. Computat. Sci.*, 2022, **61**, pp 1–27.

[25] Zedadra, O., Guerrieri, A., Jouandeau, N., Spezzano, G., Seridi, H. and Fortino, G. Swarm intelligence-based algorithms within IoT-based systems: A review, *Journal of Parallel and Distributed Computing*, 2018, **122**, pp 173–187.
[26] Mavrovouniotis, M., Li, C. and Yang, S. A survey of swarm intelligence for dynamic optimisation: Algorithms and applications, *Swarm Evol. Comput.*, **20167**, 33, pp 1–17.
[27] Khishe, M. and Mosavi, M.R. Chimp optimisation algorithm, *Expert Syst. Appl.*, 2020, **149**, pp 1–26.
[28] Kharrich, M., Mohammed, O.H., Kamel, S., Aljohani, M., Akherraz, M. and Mosaad, M.I. Optimal design of microgrid using chimp optimisation algorithm, 2021 IEEE International Conference on Automation/XXIV Congress of the Chilean Association of Automatic Control (ICA-ACCA), 2021, pp 1–5.
[29] Fathy, A., Yousri, D., Abdelaziz, A.Y., and Ramadan, H.S. Robust approach based chimp optimisation algorithm for minimizing power loss of electrical distribution networks via allocating distributed generators, *Sustain. Energy Technol. Assessm.*, 2021, **47**, pp 1–18.
[30] Essam, H., Emam, M.M. and Ali, A.A. An efficient multilevel thresholding segmentation method for thermography breast cancer imaging based on improved chimp optimisation algorithm, *Expert Systems with Applications*, 2021, **185**, pp 1–18.
[31] Hu, T., Khishe, M., Mohammadi, M., Parvizi, G.R., Taher Karim, S.H. and Rashid, T.A. Real time COVID-19 diagnosis from X-Ray images using deep CNN and extreme learning machines stabilized by chimp optimisation algorithm, *Biomed. Sig. Proc. Contr.*, 2021, **68**, (15), pp 1–17.
[32] Zhang, T., Yan, X., Huang, W., Che, X., Wang, Z. and Lu, En. Design and analysis of the air-breathing aircraft with the full-body wave-ride performance, *Aerosp. Sci. Technol.*, 2021, **119**, (15), pp 1–10.
[33] Keshmiri, S. and Colgren, R. Six-DOF modeling and simulation of a generic hypersonic vehicle for control and navigation purposes, Collect. Tech. Pap. - AIAA Guid. Navig. Control Conf., 2006, **7**, pp 4680–4689.
[34] Williams, P., Sun, R.S., Bai, H.Y. and Yan, D.W. Application of pseudo-spectral methods for receding horizon control, *J. Guid. Contr. Dynam.*, 2004, **29**, (2), pp 310–314.

Cite this article: Zhang X., Yan J., Liu S. and Yan B. (2023). Enhancing the take-off performance of hypersonic vehicles using the improved chimp optimisation algorithm. *The Aeronautical Journal*, **127**, 737–753. https://doi.org/10.1017/aer.2022.70